

Undrained shearing response of loose sand subjected to different strain paths addressing evolution of fabric anisotropy and non-coaxiality

Adil Nazir¹, and Mousumi Mukherjee^{1,*}

¹School of Civil and Environmental Engineering, Indian Institute of Technology Mandi, India

Abstract. The undrained shearing response of loose sand usually depicts a sudden loss in shear strength due to emergence of liquefaction type solid-fluid instability. For real field cases, such solid-fluid instability leads to catastrophic failure of geotechnical structures resulting in loss of life and property. In such cases, the loading is generally displacement/strain controlled with existence of a generalized strain state. Consequently, consideration of various strain paths becomes crucial while analysing the mechanical response of saturated loose sand subjected to undrained shearing. Furthermore, due to distinct evolution of fabric structure, granular materials like sand exhibits significant variation in its mechanical response when sheared under different loading paths. In this regard, 3D Discrete Element simulations of constant volume true-triaxial test have been carried out on loose sand specimen mimicking the undrained shearing condition at varying intermediate principal strain ratios (b_ε). The effect of b_ε on the macro-level response, including stress-strain behavior, stress path and pore-water pressure evolution have been investigated. Further, such macro-level responses are examined in light of the evolving fabric anisotropy. The simulation results indicate a reduction in the liquefaction susceptibility with increasing b_ε . Additionally, non-coaxiality between macro-level stress, strain and micro-level fabric has also been investigated in the present study.

1 Introduction

Sand, being inherently granular, exhibits significant variation in its mechanical response when sheared under different loading paths, primarily due to distinct evolution of the fabric structure. Such fabric structure significantly impacts the strength and deformation characteristics of the granular materials [1]. Owing to such granular structure, sand also exhibits noticeable non-coaxiality in macro-level stress-strain response during such shearing process. While shearing saturated loose sand under undrained boundary condition, a decrease in the shear strength is usually noticed due to increase in the pore-water pressure, which further leads to solid-fluid instability like static liquefaction phenomenon [2]. Shearing under such cases is generally displacement/strain controlled and hence, consideration of various strain paths becomes crucial while analysing the mechanical response of saturated loose sand subjected to undrained shearing. It is to be noted that few studies have looked into the evolution of fabric structure during undrained shearing along various loading paths [3]. Further, the evolution of such fabric structure, and non-coaxiality between the macro-level response and micro-level attributes have not been investigated during undrained shearing of loose sand along different strain paths. In this regard, Discrete Element Method (DEM) based micro-mechanical analysis can be very useful to investigate the effect of different strain paths on the

manifestation of undrained shear strength in loose sand with a particular focus on the role of fabric anisotropy and associated changes in the non-coaxiality condition.

In the present study, 3D DEM simulations of constant volume true-triaxial test have been carried out on loose sand specimen mimicking the undrained shearing condition at varying intermediate principal strain ratios (b_ε). First, the effect of b_ε on the macro-level response, including stress-strain behavior, stress path and pore-water pressure evolution have been investigated. Next, such macro-level responses are examined in light of the evolving fabric anisotropy. Further, the non-coaxiality between the stress, incremental strain and different fabric tensors during undrained shearing under various strain paths have been investigated through the evolution of Lode angles for stress (θ_σ), incremental strain (θ_ε), and fabric ($\theta_\phi, \theta_\Omega$) tensors, where θ_ϕ and θ_Ω represent the Lode angles corresponding to the contact normal fabric tensor and the contact normal force fabric tensor, respectively.

2 Methodology

Particle Flow Code-3D (PFC3D) have been employed in the present study to perform the DEM simulations of constant volume undrained true-triaxial test [4]. The 3D DEM model have been validated under undrained triaxial compression condition by comparing the

* Corresponding author: mousumi@iitmandi.ac.in, mousumi.ju06@gmail.com

simulation results with the experimental test of Liu et al., [5] on angular shaped Hostun sand particles. A 24 mm cube scaled down specimen with six frictionless walls has been adopted in the DEM simulation as shown in Fig. 1 (a). The grain size distribution of the Hostun sand specimen has been shown in Fig. 1 (b), where percentage of particle finer (passing) than a given size (diameter) is plotted, and it has a mean particle diameter (d_{50}) of 0.935 mm. A total of 20,315 spherical particles has been randomly generated within the specimen. In order to indirectly capture the shape effect of angular shaped Hostun sand particles, a rolling resistance type linear contact model have been employed [4]. Upon calibration with experimental result of Liu et al. [5], interparticle rolling (μ_r) and friction coefficient (μ_s) during shearing has been obtained as 0.8 and 0.46, respectively. Further, particle density of 2500 kg/m³ has been used with an effective Young's modulus (E^*) of 3.0×10^8 Pa and normal to shear stiffness ratio (k^*) of 35. Based on E^* and k^* , normal (k_n) and shear stiffness (k_s) of particles can be calculated as

$$k_n = AE^*/L \quad (1)$$

$$k_s = k_n/k^* \quad (2)$$

Where, for a given contact, A is the projected area of the sphere having smaller radius, L is the distance between the centres of two spheres in case of ball-ball contact or radius of the sphere in case of ball-wall contact.

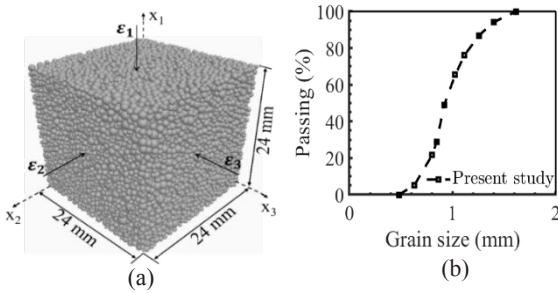


Fig 1. (a) Schematic of true triaxial test (walls excluded), (b) grain size distribution adopted in the DEM simulation.

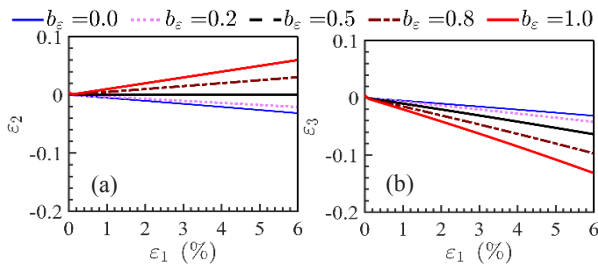


Fig 2. Evolution of (a) intermediate (ϵ_2) and (b) minor principal strain (ϵ_3).

The constant volume DEM simulations of true-triaxial test have been conducted on a loose specimen with initial void ratio of 0.7788 under an initial mean confinement of 100 kPa and μ_r value of 0.8. This pre-shearing void ratio has been achieved by keeping $\mu_s = 0.4$ during the isotropic compression stage. In the subsequent shearing stage, μ_s has been changed to the calibrated value of 0.46. The influence of different strain paths ($b_\epsilon = 0.0, 0.2, 0.5, 0.8, 1.0$) has been assessed by keeping the intermediate strain ratio ($b_\epsilon = \Delta\epsilon_2 - \Delta\epsilon_3 / \Delta\epsilon_1 - \Delta\epsilon_3$) constant during shearing. For a

given b_ϵ , ϵ_1 is compressive; whereas, ϵ_2 and ϵ_3 alter in such a way that the volume of the specimen remains constant (Fig 2). Under the plane strain condition, which corresponds to $b_\epsilon = 0.5$, ϵ_2 remains constant at zero; whereas, ϵ_1 and ϵ_3 change at a same rate but in the opposite direction. Further, the shearing has been conducted at an axial strain rate of 0.09/s maintaining a quasi-static condition, which is ensured by the condition of non-dimensional inertial number, $I < 10^{-3}$ [3].

3 Results and discussion

3.1 Macro-level stress manifestations and micro-level fabric evolution

The macro-level response has been assessed in terms of deviatoric stress q , effective mean stress p' , pore-water pressure u and principal effective stresses σ'_i ; whereas, micro-level response has been assessed in terms of geometrical coordination number Z_g and principal contact normal fabric ϕ which are defined as:

$$Z_g = 2N_c / (N - N_0) \quad (3)$$

$$\phi = \sum_{c \in N_c} (n_i n_j) / N_c \quad (4)$$

Where, N_c is total number of interparticle contacts, N is total number of particles, N_0 number of particles with zero contacts and \mathbf{n} is unit contact normal vector.

Figure 3(a, b, c) depicts the evolution of macro-level undrained response of sand pertaining to different strain paths. It has been observed from Fig. 3(a, b) that for $b_\epsilon \leq 0.5$, loose sand shows complete static liquefaction phenomenon; whereas, for $b_\epsilon > 0.5$, it exhibits temporary liquefaction with an initial peak in the deviatoric stress response. Further, it can be observed that with increase in b_ϵ , the axial strain at peak deviatoric stress (or initial peak for $b_\epsilon > 0.5$) decreases as depicted in Fig. 4a. However, the peak deviatoric stress slightly increases with b_ϵ for the condition $b_\epsilon \leq 0.5$; whereas, such initial peak exhibits a decreasing trend for $b_\epsilon > 0.5$ as depicted in Fig. 4b. This can be explained through the pore-water pressure response noted during the shearing as presented in Fig. 3c. It has been observed that at low strain level (1 – 2%), the rate of generation of excess pore-water pressure is quite high for $b_\epsilon > 0.5$, which results a decrease in the manifestation of effective mean stress and subsequent decrease in the initial peak deviatoric stress. However, for $b_\epsilon \leq 0.5$, very small variation has been noted for the pore pressure response, resulting in slight increase of peak deviatoric stress with increasing b_ϵ . On the contrary, at the higher axial strain level ($> 2\%$), with increasing b_ϵ a consistent decrease in the pore-water pressure generation is evident with shearing, which results into reduced liquefaction susceptibility. This is consistent with the micro-level observation, i.e. evolution of the average number of contacts, which is evaluated using geometrical coordination number, Z_g and average contact normal force, F_N^{avg} as depicted in Fig 3(d, e), respectively. For specimen exhibiting complete liquefaction, it can be observed that Z_g and F_N^{avg} show a sudden drop with F_N^{avg} attaining a zero value at complete static liquefaction. With further continued shearing Z_g

increases due to progressive rearrangement of fabric; whereas, F_N^{avg} value remains constant at zero indicating no stress increase after complete static liquefaction (Fig. 3b). At the higher axial strain level ($> 2\%$), Z_g and F_N^{avg} can be noted to increase markedly with increasing b_ε . As a result, enhanced deviatoric stress has been noticed at higher axial strain level, which manifests resistance against complete liquefaction. However, Z_g and F_N^{avg} are inadequate in providing complete information about the directional dependency of the contacts, which is useful for investigating the effect of different intermediate principal strain paths. In this regard, the evolution of contact normal fabric components can be crucial in extracting meaningful insights.

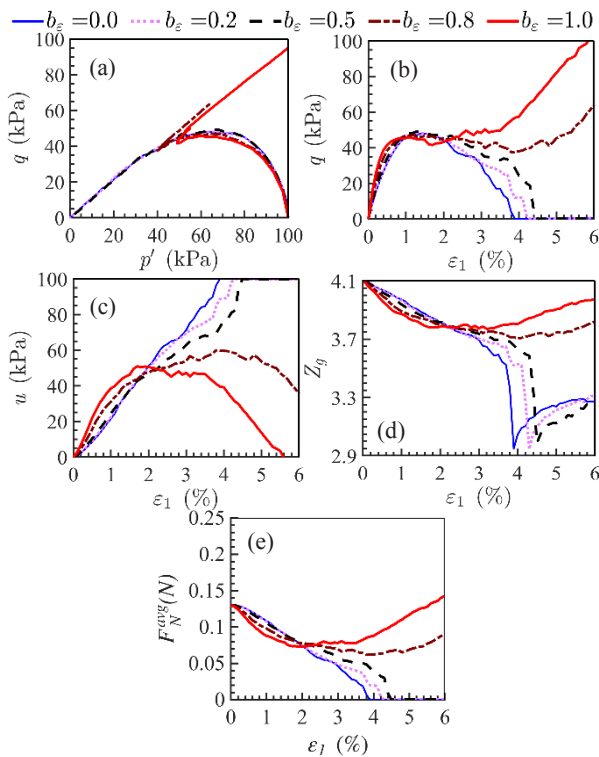


Fig 3. Evolution of macro-level (a) stress path, (b) deviatoric stress (q), (c) pore-water pressure (u), (d) geometrical coordination number (Z_g) and (e) average contact normal force (F_N^{avg}) during the undrained shearing.

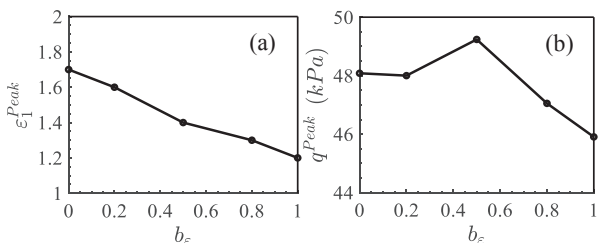


Fig 4. (a) Axial strain at peak deviatoric stress and (b) recorded peak deviatoric stress during shearing at different b_ε values.

Figure 5 depicts the evolution of principal contact normal fabric and principal stress related to different strain paths. It can be observed that the evolution of major principal fabric, Φ_1 exhibits an increasing trend with shearing, while its value is lower for higher b_ε values. Similarly, Φ_3 values are also noticed to be lower for higher b_ε values; however, it exhibits a decreasing

trend during shearing. On the contrary, the evolution Φ_2 exhibits both increasing and decreasing trend for $b_\varepsilon > 0.5$ and $b_\varepsilon < 0.5$, respectively. However, unlike Φ_1 and Φ_3 , Φ_2 has been observed to be higher with increasing b_ε . At higher strain level, the respective increase noticed in the Φ_1 and Φ_2 components for the cases with $b_\varepsilon > 0.5$ indicates enhanced contacts in the major and intermediate principal directions resulting in increased principal stresses as depicted in Fig 5(b, d). Eventually, the combined increase in these principal stress components results into an enhanced effective mean stress at higher b_ε values, which translates to a higher deviatoric shear stress and liquefaction resistance.

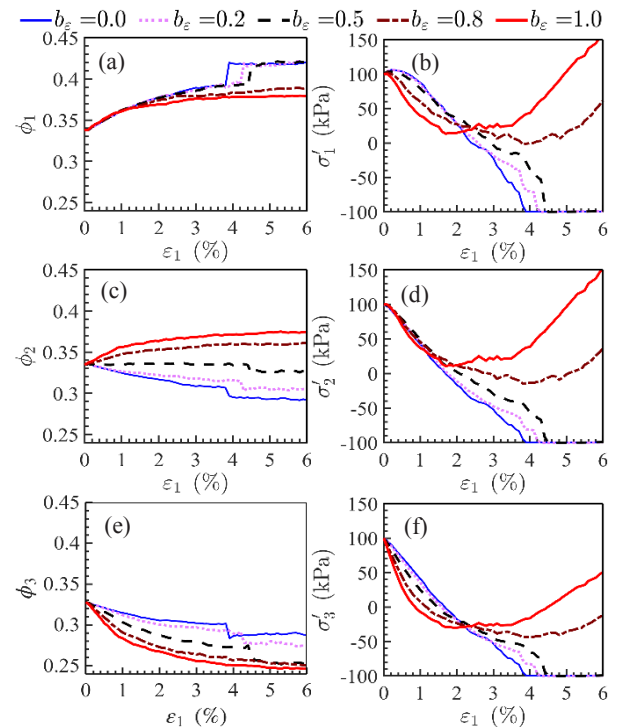


Fig 5. Evolution of principal (a, c, e) fabric and (b, d, f) stress components.

3.2 Non-coaxiality in stress, strain and fabric

As the eigen-directions of any tensor can be quantitatively assessed in the π plane by the Lode angle θ , the non-coaxiality has been investigated in the present study by comparing the differences between the Lode angles of stress (θ_σ), incremental strain (θ_ε), contact normal fabric (θ_ϕ) and contact normal force fabric (θ_Ω) tensors. The Lode angle of a tensor σ defines the angle between the major principal direction and the second invariant of the deviatoric part of the σ tensor in the π plane, and is estimated using the following relation

$$\theta_\sigma = \tan^{-1}[\sqrt{3}(\sigma_2 - \sigma_3)/(2\sigma_1 - \sigma_2 - \sigma_3)] \quad (5)$$

$$\theta_\sigma = \tan^{-1}[\sqrt{3}(b_\sigma)/(2 - b_\sigma)] \quad (6)$$

$$b_\sigma = (\sigma_2 - \sigma_3)/(\sigma_1 - \sigma_3) \quad (7)$$

Where, σ_1 , σ_2 and σ_3 are the major, intermediate, and minor principal values, and b_σ is the intermediate ratio corresponding to tensor σ .

Figure 6 depicts the evolution of $(\theta_\sigma - \theta_\varepsilon)$, $(\theta_\Omega - \theta_\phi)$, $(\theta_\varepsilon - \theta_\phi)$ and $(\theta_\sigma - \theta_\Omega)$ for varying strain paths (b_ε values). It can be noticed that initially, stress and

incremental strain tensors are nearly coaxial across all the strain paths ($\theta_\sigma - \theta_\varepsilon < -5^\circ$). However, with continued shearing, stress and incremental strain tensors remain coaxial only in case of axisymmetric strain paths ($b_\varepsilon=0$ and $b_\varepsilon=1$), and progressively become non-coaxial ($\theta_\sigma - \theta_\varepsilon > -5^\circ$) for the non-axisymmetric strain paths ($0 < b_\varepsilon < 1$), mainly due to the gradual reduction in the b_σ value. Furthermore, contact normal fabric and contact normal force fabric tensors are also nearly coaxial ($\theta_\Omega - \theta_\phi < -5^\circ$) for axisymmetric strain paths except at low strain level; whereas, for the non-axisymmetric strain paths it is non-coaxial ($\theta_\Omega - \theta_\phi > -5^\circ$) for major part of the shearing. Nonetheless, noticeable coaxiality exists between the incremental strain and contact normal fabric tensors ($\theta_\varepsilon - \theta_\phi < \pm 5^\circ$), and between the stress and contact normal force fabric tensors ($\theta_\sigma - \theta_\Omega < \pm 5^\circ$) at higher axial strain level. These non-coaxial responses among the stress, strain, and fabric tensors are consistent with the observations reported in the earlier DEM studies incorporating various intermediate stress paths [1]. Further comparing different strain paths, it can be noticed that non-coaxiality is significant for plane strain condition ($b_\varepsilon = 0.5$) at higher axial strain level, as the component of strain pertinent to intermediate direction is fixed; whereas, the stress and fabric tensor components can freely evolve in the intermediate direction.

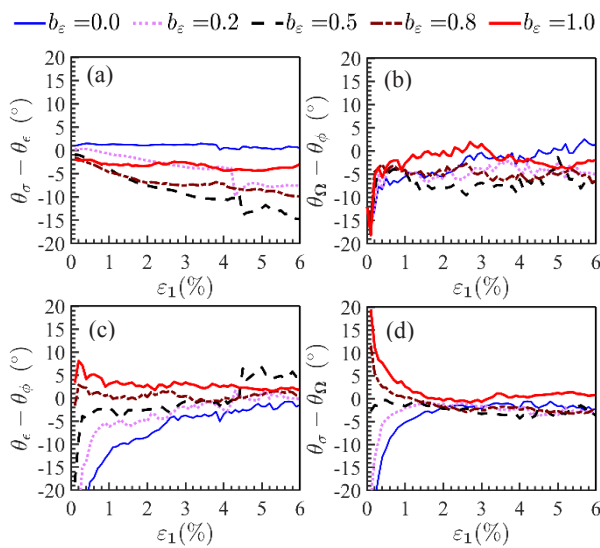


Fig 6. Evolution of differences between the Lode angles corresponding to (a) stress and incremental strain tensors ($\theta_\sigma - \theta_\varepsilon$), (b) contact normal force fabric and contact normal fabric tensors ($\theta_\Omega - \theta_\phi$), (c) strain and contact normal fabric tensors ($\theta_\varepsilon - \theta_\phi$), and (d) stress and contact normal force fabric tensors ($\theta_\sigma - \theta_\Omega$).

4 Conclusion

A series of undrained true-triaxial test has been performed on Hostun sand using constant volume 3D DEM simulations to investigate the micro-mechanics associated with the shearing along different strain paths. Isotropic assemblies have been prepared under loose density state to investigate the undrained shearing response under five different b_ε values. An assembly of

spherical shaped particle has been generated, where the shape effect has been captured by rolling resistance model. The micro-mechanical parameters corresponding to Hostun sand have been calibrated using the experimental data of undrained triaxial compression test reported in the literature.

It has been observed that a reduction in the liquefaction susceptibility is evident with increase in the b_ε values, where complete liquefaction takes place for the range $0 \leq b_\varepsilon \leq 0.5$ and limited liquefaction with a phase transformation occur beyond $b_\varepsilon = 0.5$. In case of complete liquefaction ($0 \leq b_\varepsilon \leq 0.5$), undrained shear strength has been noticed to increase with b_ε values. Conversely, for the case of limited liquefaction ($b_\varepsilon \geq 0.5$), the initial peak shear stress decreases with increasing values of b_ε . Such change in the liquefaction susceptibility with increasing b_ε is attributed to the enhanced contribution of the intermediate principal fabrics, which imparts higher effective mean stress by inducing additional intermediate principal stress. It has also been noticed that coaxiality exists between stress and incremental strain tensors at low axial strain level. However, with continued shearing, non-coaxiality is clearly visible between the stress and incremental strain tensors in case of non-axisymmetric strain paths and coaxiality exists only for the axisymmetric strain paths. While further comparing the evolution of the stress, incremental strain and fabric tensors, coaxiality has been observed between the strain and contact normal fabric tensors, and between the stress and contact normal force fabric tensors at higher axial strains. However, comparison of contact normal fabric and contact normal force fabric tensors reveals coaxial response for axisymmetric strain paths only; whereas, non-coaxiality is evident in case of non-axisymmetric strain paths for majority of the shearing process.

The authors would like to acknowledge Dr. Arghya Das from IIT Kanpur, India for providing access to the PFC 3D software.

References

1. Liu, Y., Zhang, D., Wu, S., Yu, P.: DEM Investigation on the Evolution of Fabric under True Triaxial Conditions in Granular Materials. *Int. J. Geomech.* 20, 1–13 (2020).
2. Yamamuro, J.A., Lade, P. V.: Static liquefaction of very loose sands. *Can. Geotech. J.* 34, 905–917 (1997).
3. Salimi, M.J., Lashkari, A.: Undrained true triaxial response of initially anisotropic particulate assemblies using CFM-DEM. *Comput. Geotech.* 124, 103509 (2020).
4. Itasca (2008) PFC3D, Particle Flow Code in 3 Dimensions, User's Guide. 4th Edition. - References - Scientific Research Publishing.
5. Liu, Y.-J., Li, G., Yin, Z.-Y., Dano, C., Hicher, P.-Y., Xia, X.-H., Wang, J.-H., Bauer, E., Behringer, R.P., Darve, F., Kondic, L.: Influence of grading on the undrained behavior of granular materials. *Comptes Rendus Mec.* 342, 85–95 (2014).